RESEARCH ARTICLE

JOURNAL OF morphology WILEY

Correlated evolution of beak and braincase morphology is present only in select bird clades

Xiaoni Xu[1] 🄳 | Rossy Natale[2] 🄳

[1]Department of Organismal Biology and Anatomy, University of Chicago, Chicago, Illinois, USA

[2]Cornell Lab or Ornithology, Cornell University, Ithaca, New York, USA

Correspondence
Rossy Natale, Cornell Lab or Ornithology, Cornell University, Ithaca, NY 14850, USA.
Email: rnn22@cornell.edu

Xiaoni Xu, Department of Organismal Biology and Anatomy, University of Chicago, Chicago, IL 60637, USA.
Email: xiaoni@uchicago.edu

Abstract

Complex morphological structures, such as skulls or limbs, are often composed of multiple morphological components (e.g., bones, sets of bones) that may evolve in a covaried manner with one another. Previous research has reached differing conclusions on the number of semi-independent units, or modules, that exist in the evolution of structures and on the strength of the covariation, or integration, between these hypothesized modules. We focus on the avian skull as an example of a complex morphological structure for which highly variable conclusions have been reached in the numerous studies analyzing support for a range of simple to complex modularity hypotheses. We hypothesized that past discrepancies may stem from both the differing densities of data used to analyze support for modularity hypotheses and the differing taxonomic levels of study. To test these hypotheses, we applied a comparative method to 3D geometric morphometric data collected from the skulls of a diverse order of birds (the Charadriiformes) to test support for 11 distinct hypotheses of modular skull evolution. Across all Charadriiformes, our analyses suggested that charadriiform skull evolution has been characterized by the semi-independent, but still correlated, evolution of the beak from the rest of the skull. When we adjusted the density of our morphometric data, this result held, but the strength of the signal varied substantially. Additionally, when we analyzed subgroups within the order in isolation, we found support for distinct hypotheses between subgroups. Taken together, these results suggest that differences in the methodology of past work (i.e., statistical method and data density) as well as clade-specific dynamics may be the reasons past studies have reached varying conclusions.

KEYWORDS
Charadriiformes, geometric morphometrics, integration, macroevolution, modularity

Xiaoni Xu and Rossy Natale should be considered joint first authors.

1 | INTRODUCTION

The patterns defining the morphological evolution of complex or diverse structures have long been of interest in evolutionary biology. In particular, how the correlated evolution of different anatomical units may relate to the phenotypic space available to a species or to the rate of diversification in morphological structures are common questions (e.g., Navalón et al., 2020) in regard to morphological evolution. This idea is encapsulated by the term integration which, in the context of evolutionary morphology, describes the correlated evolution of traits within clades (Zelditch & Goswami, 2021). Differences in the degree of integration within and between different morphological features generate evolutionary modularity: the semi-independent evolution of sets of traits (Klingenberg, 2008). A greater degree of modularity represents stronger evolutionary covariation between individual components within a module relative to the associations between modules (Adams & Collyer, 2019). Modularity is often examined in the context of other factors, such as diversification rates to provide insight into the mechanisms governing the diversification of complex morphological structures. For example, Larouche et al. (2018) found support for modular evolution across the bodies of ray-finned fishes and, by analyzing body shape evolution in a phylogenetic context, were able to make predictions about how increased modularity may facilitate rapid morphological diversification.

The vertebrate skull has been a focus of research on evolutionary modularity due to its heterogeneous developmental origins (Couly et al., 1993) and its multiple roles in biomechanical (e.g., feeding on different food items; Vidal García & Scott Keogh, 2017) and sensory systems (e.g., vision; Heesy, 2008). Morphometric data have been used to test support for different modularity hypotheses across the skulls of diverse clades, including amphibians (Bardua et al., 2019; Bon et al., 2020), mammals (Adams & Collyer, 2019; Goswami & Finarelli, 2016), and birds (Klingenberg & Marugán-Lobón, 2013). These studies have found support for modular hypotheses of varying complexities, with studies often recovering the strongest support for hypotheses with a large number of semi-independent skull modules. For example, Watanabe et al. (2019) found support for a hypothesis in which the skulls of lizards and snakes evolved as 10 and 9 semi-independent modules, respectively, while analyses by Bardua et al. (2020) suggest an even more complex 13 module patterns in frog skull evolution. These findings suggest that the patterns of modular evolution vary across clades of vertebrates, but may often involve finely subdivided parts of the skull evolving semi-independently from one another.

Underlying these studies of modularity are often interests in understanding how the semi-independent evolution of anatomical regions may relate to the generation of ecologically important morphological diversity. It has been hypothesized that the pronounced variation in avian beak shape (Cooney et al., 2017) may have been facilitated by its semi-independent evolution from the rest of the avian skull. Application of partial least squares (PLS) analysis, as well as calculations of RV coefficients on two-dimensional landmark points from the skulls (excluding the distal portion of the beak) from 160 species of birds, suggests that the avian skull has evolved as an integrated unit (Klingenberg & Marugán-Lobón, 2013). Similar findings have been suggested using PLS on smaller taxonomic subsets with support recovered for integrated evolution between two subsets of landmarks delimiting the beak from the rest of the skull in analyses on six corvid species (Kulemeyer et al., 2009), on 147 species of birds of prey (Bright et al., 2016), and on 170 species of parrots and cockatoos (Bright et al., 2019).

Finding support for integrated evolution does not necessarily rule out semi-independent evolution between modules. In other words, it is possible for morphological components to evolve in an integrated manner but with certain regions still evolving semi-independently from one another (Drake & Klingenberg, 2010). More recently developed methods (e.g., Goswami & Finarelli, 2016 and Adams & Collyer, 2019) allow us to quantify the strength of covariation between modules under any given hypothesis while allowing for direct comparisons of the support for the different modularity hypotheses. The ability to compare multiple, sometimes similar hypotheses is particularly useful given that, depending on where landmarks are placed, the delineations of what landmarks should be ascribed to a hypothesized module (particularly for landmarks that are placed along borders) are not necessarily clear. To date, studies of bird clades using these methods have yielded highly variable results. Using a high-resolution geometric morphometric data set with a likelihood-based approach (evaluating modularity with maximum likelihood: EMMLi, Goswami & Finarelli, 2016), Felice and Goswami (2018) found that, of the 16 different modularity hypotheses assessed, a seven-module hypothesis was best supported across a broad phylogenetic sample of 352 bird species. However, it has recently been noted that EMMLi appears to have high type I error rates, and a tendency to overfit modular hypotheses compared to a newer method for evaluating modularity hypotheses based on an effect size measure (Adams & Collyer, 2019). Given this disagreement on whether avian skull evolution has been characterized by modular evolution or not, it is imperative to reevaluate modular patterns in a nuanced framework.

We used detailed three-dimensional data and recently developed methods to evaluate support for different hypotheses of modularity in an ecologically and morphologically diverse order of birds: the Charadriiformes. Charadriiformes encompasses ~370 species of sand pipers, plovers, gulls, and their relatives. Ecological diversity within the order is high and reflected in their skull morphology, especially in the beak (Moreno, 1999). For example, while common ringed plovers (Charadrius hiaticula) have small, stout skulls that are adapted to surface pecking, long-billed curlews (Numenius americanus) have extremely long and curved skulls that are used to probe soft sediments for prey (del Hoyo et al., 1996), and Atlantic puffins (Fractercula arctica) have deep beaks and wide skulls that they use to capture fish while diving underwater (Lowther et al., 2020). This morphological diversity, combined with the availability of a comprehensive, well-resolved, time-calibrated phylogeny (Černý & Natale, 2022), makes Charadriiformes a good model for studying the evidence for covariation between avian skull components during their evolution. Using data describing skull morphologies of 262 out of ~370 extant species of Charadriiformes, we assessed support for a set of 11 modularity hypotheses at both the ordinal and subgroup level while simultaneously assessing how varying the density of our 3D landmark data impacted our results. We

recovered the strongest support for a two-module modularity hypothesis where the beak evolves semi-independently from, but still in a correlated manner with, the rest of the skull. Additionally, we find evidence that the support for this hypothesis is largely driven by one subgroup, with the other subgroup examined exhibiting unique evolutionary dynamics. Our results highlight key methodological considerations and suggest a framework in which future modularity research may operate.

2 | MATERIALS AND METHODS

2.1 | Morphological data collection and visualization

Morphological data was taken from Natale and Slater (2022). This data set comprises 255 three-dimensional landmarks (42 landmarks placed at discrete locations, 213 semi-landmarks) taken from 262 species (represented by over 400 individual specimens) of Charadriiformes. These landmarks were placed on all portions of the skull (see Figure 1), with relatively dense semi-landmarks placed along the sides and tops of the beak to limit the Pinocchio effect (Walker, 2000; Zelditch et al., 2004), where a distant landmark (e.g., tip of the beak) can cause spurious results in analyses. All landmarks were digitized using Stratovan Checkpoint (Stratovan Corporation, 2018) from three-dimensional surface scans that capture the external bony morphology of skulls housed in museum skeletal collections. For further details on scan settings, digitization, and landmark processing, we refer readers to Natale and Slater (2022). A full list of the specimens used in our analysis is available in the supplementary online material in Table 1. All analyses were run in R (RStudio Team, 2019) unless otherwise noted.

Goswami et al. (2019) noted that variation in the density of landmark placement might lead to different outcomes when testing modularity hypotheses. To assess the sensitivity of our results to changes in the density and spread of morphometric data, all ordinal level analyses were conducted on three landmark sets representing three different densities of landmarks (Figure 1): The full set of 255 landmarks, an intermediate density set of 154 landmarks (42 landmarks placed at discrete locations, 112 semi-landmarks), and a low density set of 113 landmarks (38 landmarks placed at discrete locations, 75 semi-landmarks). The three distinct densities of landmarks predominantly differed in the number of semi-landmarks placed along the curves (Figure 1), but the lowest density landmark set also contained four fewer type I landmarks (see Supplementary File, Table 2 for details). Before analyses, we slid all semi-landmarks using the slider3d function in the R (RStudio Team, 2019) package Morpho Schlager (2017) and performed Procrustes superimposition using the procSym function, also from the Morpho package, to remove the effects of size, translation, and orientation. To better interpret the results of the following sections and to understand the breadth of charadriiform skull shapes, we also performed a principal components analysis on the Procrustes aligned landmark data for the whole skull using the procSym function in the Morpho package (Schlager, 2017).
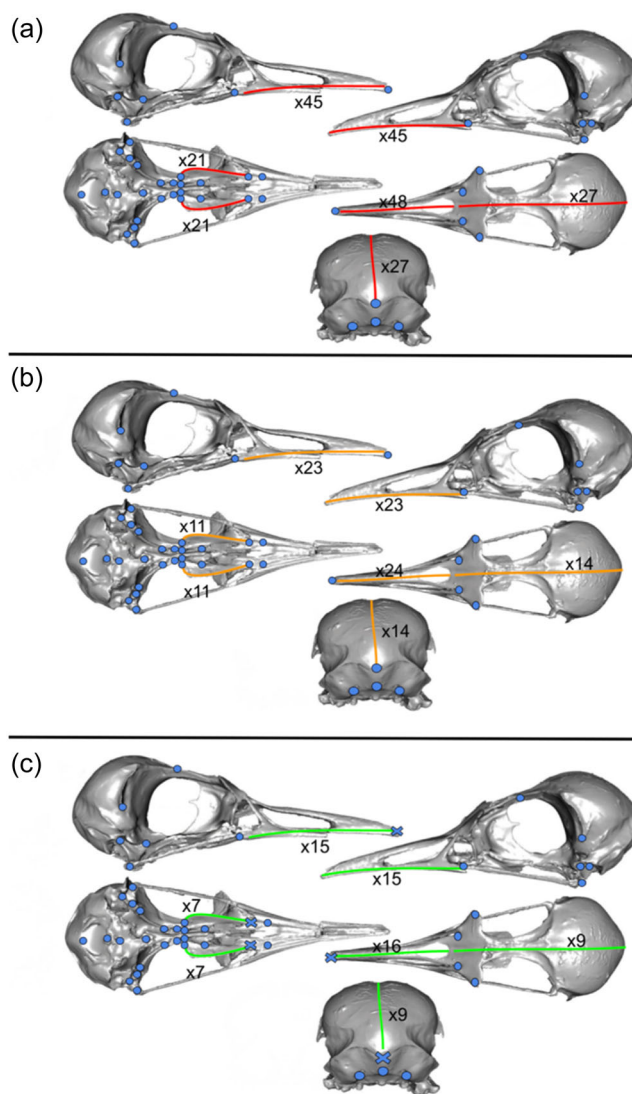

FIGURE 1 The (a) high, (b) intermediate, and (c) low density landmark schemes used in these analyses depicted on a surface scan of a least tern *Sterna antillarum* (FMNH 376281) skull. Blue dots indicate type I landmarks that are identical under each of the three different densities, with the exception of the low density (panel c) which contains four less type I landmarks that are marked with a blue 'X'. The red, orange, and green lines indicate the placement of type II (sliding semi-landmarks) at full (red), intermediate (orange), and low (green) densities. The number along each line indicates the number of semi-landmarks placed along that curve under the three distinct densities. A full description of landmarks is available in the supplementary online material, Table 2. Figure adapted from Natale and Slater (2022).

2.2 | Phylogeny

We used the charadriiform phylogeny from Černý and Natale (2022). Full details regarding the inference of this tree are available there. Briefly, the tree was generated from a supermatrix of previously published molecular sequences (12 nuclear, 15 mitochondrial) taken from GenBank (Benson et al., 2013) and a 69-character morphological data set from Chu (1995). RaXML (Stamatakis, 2014) was used to generate a maximum likelihood

topology, which was then time-scaled in the program mcmctree (Yang, 2007) using 14 fossil calibrations and a relaxed uncorrelated molecular clock. Before our analyses, we removed tips from the tree that were not present in our morphological data set using the drop.tip function from the R package ape (Paradis et al., 2020).

TABLE 1 Descriptions of each of the 11 modularity hypotheses compared. The abbreviation used for each hypothesis is given in the lefthand column with the number inside the parenthesis following each name denoting the number of modules in that hypothesis.

Hypothesis	Modules
FG (7)	[F,O, Po][Fm][B][Pl][Pt][Q][J, Pm]
FG1 (7)	[F(part),O, Po][Fm][B][Pl][Pt][Q][F(part),J, Pm]
FG2 (8)	[F(part),O, Po][Fm][B][Pl][Pt][Q][F(part)][J, Pm]
FG3 (5)	[F,O, Po, Fm,J, Pm][B][Pl][Pt][Q]
FG4 (4)	[F,O, Po, Fm,B,J, Pm][Pl][Pt][Q]
FG5 (5)	[F,O, Po,B,J, Pm][Fm][Pl][Pt][Q]
FG6 (5)	[F,O, Po][Fm,B,J, Pm][Pl][Pt][Q]
FG7 (8)	[F,O][Po][Fm][B][Pl][Pt][Q][J, Pm]
FG8 (9)	[F,O][Po][Fm][B][Pl][Pt][Q][J][Pm]
BKBR1 (2)	[F,O, Po, Fm,B][Pl, Pt,Q,J, Pm]
BKBR2 (2)	[F,O, Po, Fm,B, Pl, Pt,Q,J][Pm]

Note: These descriptions refer to the beak and braincase Hypothesis 1 (BKBR1), beak and braincase Hypothesis 2 (BKBR2), the Felice Goswami (FG) hypothesis, and its eight variations (FG1, FG2, etc.). The righthand column includes hypothesized modules, separated by brackets, with the bones included in each hypothesized module given by distinct letter codes. See Figure 3 for the letter codes used here.

2.3 | Modularity hypotheses

We assessed support for a total of 11 distinct modularity hypotheses (Figure 2, see Figure 3 for a legend noting the different bones in the avian skull). These hypotheses can be broadly divided into two groups. The first involves variations on the seven-module hypotheses of Felice and Goswami (2018). We did not include the nasal module in this original seven-module hypothesis as its structure cannot be reliably found across the surface scans we used here. Therefore, we instead adopted a similar version to their original Felice and Goswami (2018) model, adjusting for our methodological choices (i.e., differing landmark placements, keeping the quadrate and pterygoid as separate modules). We tested support for this modified hypothesis and eight variations of it based on the relatively complex, seven-module version by Felice and Goswami (2018). Hereafter, we refer to the first version of this hypothesis as the Felice Goswami (FG) hypothesis with the variations on this hypothesis labeled sequentially {FG1, FG2,..., FG8}. Secondly, we assessed support for two variations of a relatively simpler 'beak and braincase model' (hereafter referred to as the BKBR1 and BKBR2 hypotheses) that have been suggested in previous work (e.g., Bright et al., 2016). Variations on both of these hypotheses were generated by altering groupings of landmarks based on either knowledge of the functional interactions (e.g., the quadrate does not touch the palate bones, but is functionally linked during mouth opening and closing; Olsen & Westneat, 2016) or proximity between different parts of the skull (e.g., the basioccipital bone is separated from the neighboring parietal bone in some hypotheses). In addition, we compared support for these 11 hypotheses to a null hypothesis, where all landmarks are considered part of one single module (i.e., no modularity).
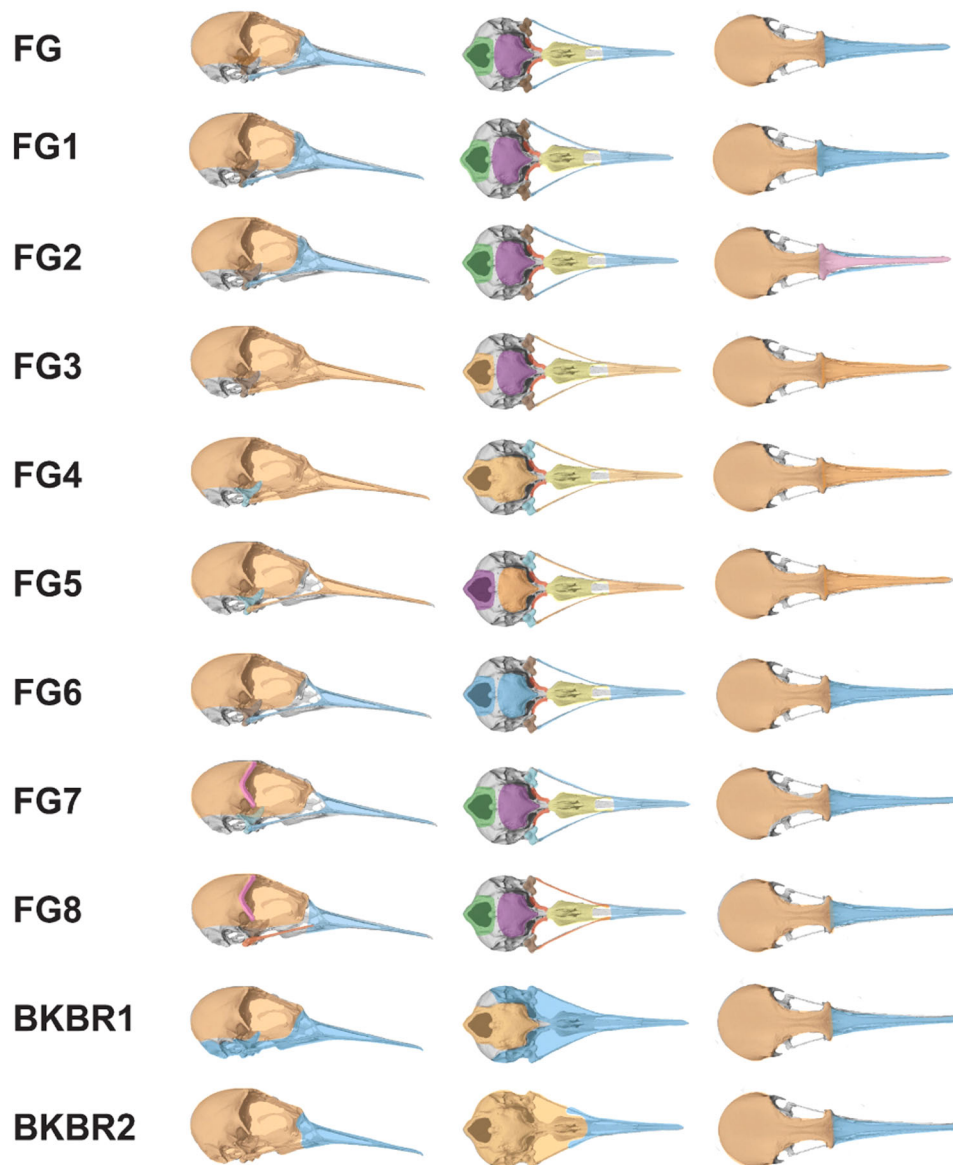
TABLE 2 CR scores, p values, and Z_{cr} scores for each modularity hypothesis tested using the full (FLL), intermediate (INT), and low (LOW) density landmark data.

Hypothesis	CR (FLL)	p (FLL)	^{z}cr (FLL)	CR (INT)	p (INT)	^{z}cr (INT)	CR (LOW)	p (LOW)	^{z}cr (LOW)
FG	0.82	.001	−3.50	0.83	.001	−3.88	0.83	.001	−3.34
FG1	0.82	.001	−3.491	0.84	.001	−3.76	0.83	.001	−3.36
FG2	0.80	.001	−4.92	0.81	.001	−4.50	0.82	.01	−3.74
FG3	0.78	.001	−4.92	0.79	.001	−4.64	0.80	.01	−4.19
FG4	0.78	.001	−4.70	0.79	.001	−4.62	0.79	.001	−4.52
FG5	0.83	.002	−3.03	0.85	.006	−2.82	0.86	.008	−2.58
FG6	0.77	.001	−4.80	0.78	.001	−4.54	0.78	.001	−4.36
FG7	0.77	.001	−4.02	0.78	.001	−5.07	0.78	.001	−4.17
FG8	0.79	.001	−4.84	0.79	.001	−5.29	0.79	.001	−4.47
BKBR1	0.83	.001	−14.28	0.85	.001	−8.93	0.86	.001	−5.97
BKBR2	0.85	.001	−19.73	0.86	.001	−11.94	0.85	.001	−7.87

Note: The CR scores indicate the degree of correlation during morphological change among the modules in any given hypothesis. CR values closer to 0 indicate high modularity with sets of landmark points evolving more independently from one another, while CR values closer to one indicate low modularity where sets of landmarks tend to evolve in a more covaried manner with one another. p values compare the observed CR to permutations to determine if the evidence for modular evolution under that hypothesis is stronger than expected by chance ($p < .05$). Zcr scores represent a measure of support (see Figure 5 for statistical comparisons of these values) for that hypothesis with more negative values representing a stronger modular signal under that hypothesis.

FIGURE 2 Depictions of the 11 different hypotheses of charadiiform modular skull evolution shown on a skull of a red knot, *Calidris canutus* (FMNH 362893). In each image, distinct colors represent distinct modules. We refer readers to Table 1 for details on each modularity hypothesis, but make a note here that certain hypotheses (e.g., FG vs. FG1) are similar, with only small differences in how the boundaries of the modules are defined. For example, FG differs from FG1 in that the landmarks on the frontal bones are included in the beak module in the FG1 scenario while they are included in the braincase modules under the FG hypothesis. The null model of no modularity is not shown here.

2.4 | Testing support for distinct hypotheses of modular evolution across all charadriiformes

We used the covariance ratio (CR), as computed in the phylo.modularity function from the R package geomorph (Adams et al., 2021; Baken et al., 2021), to quantify the degree of the modular signal under each of the 11 different hypotheses. CR quantifies modular signal by determining and comparing the covariances within and between predefined modules (Adams & Collyer, 2019). Typically, CR varies between 0 (no covariation between modules but high covariation within modules; high modularity) and 1 (strong covariation between modules relative to between modules; low

modularity), though it may theoretically exceed 1 if covariances between modules are greater than covariances within them (Adams & Collyer, 2019).

When there are more than two modules in a given hypothesis, the CR value is averaged across pairwise comparisons of modules. A permutation procedure is then used to determine if the modular signal in the data under each distinct hypothesis is stronger than expected by chance (Adams, 2016). For each analysis, we used 999 permutations to evaluate significance.

The phylo.modularity function also returns the standardized effect sizes Z_{CR} (Adams & Collyer, 2019) for each hypothesis which we used to compare support for the 11 modularity hypotheses.
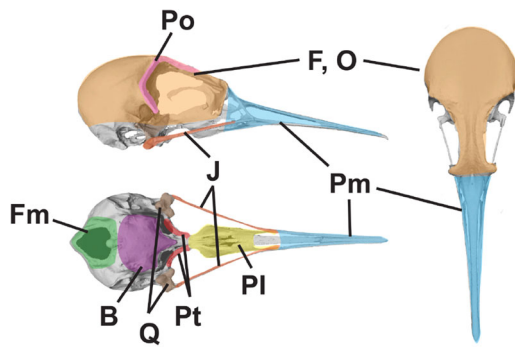
FIGURE 3 A legend of all the bones used in our analysis shown on a skull of a red knot, *Calidris canutus* (FMNH 362893). The letter codes refer to the following bones: B, basisphenoid; F, frontal; Fm, foramen magnum; J, jugal; O, occipital; Pl, palatine; Pm, premaxillary; Po, postorbital; Pt, pterygoid; Q, quadrate.

Z_{CR} evaluates the magnitude of the observed effect relative to the random outcomes of the permutation procedure used to evaluate the significance of the CR. Paired effect sizes, $\hat{Z}_{12}$, were also computed using the compare. CR function in the geomorph package (Adams et al., 2021) to allow direct comparisons of support between pairs of modularity hypotheses, including the null hypothesis of no modularity (Adams & Collyer, 2019). The compare.CR function assesses support for each hypothesis relative to one another by performing two sample Z tests on the standard error from the results of the CR permutations and will return two sample Z scores and a p value for each pairwise comparison, indicating whether there is significantly distinct support for any given hypothesis relative to another. For this reason, subgroup-level analyses were also only run using the lowest-density landmark scheme. To aid in the visualization of these morphological differences between these subgroups, we also plotted the three suborders (the Lari, Scolopaci, and Charadrii) on the morphospace generated by the principal components analysis described above.

3 | RESULTS

3.1 | Skull shape differences among charadriiformes

In our principal components analysis (Figure 4) of the full density landmark set, the first principal component (PC1) explained ~70% of the variation in shape. Negative PC1 scores correspond to elongated, narrow skulls, while positive PC1 scores correspond to skulls that are shorter and wider. The second principal component (PC2) explained ~13% of the variance. Negative PC2 scores correspond to skulls with a large angle between the beak and braincase, a more rounded braincase with large orbits, and more rostrally placed quadrates and foramen magnum. As PC2 scores increase, the skulls become flattened, such that the angle between the beak and braincase decreases, the braincase becomes flatter, and the quadrates and

foramen magnum shift caudally. The three subgroups were not equally spread across this morphospace (visualized in Figure 4). The Scolopaci and, to a lesser extent, the Charadrii tended to span the whole range of PC1 values, whereas the Lari tended to be restricted to higher PC1 values. This restriction indicates that species within the Lari tended to have shorter, wider skulls, whereas the other two suborders varied in the length and width of the skull. There was less distinction between the suborders along PC2, although the highest values along this axis were seen in the Lari. In general, there was a higher degree of overlap between the Charadrii and the Scolopaci whereas the Lari overlapped less with either suborder.

3.2 | Testing support for distinct hypotheses of modular evolution across all charadriiformes

We found that all eleven hypotheses tested received significant support ($p < .05$) relative to a null model, although the CR values for all hypotheses and all landmark densities were relatively high (all >0.76), indicating that there was a relatively high degree of covariation between modules. The strength of the modular signal under each hypothesis, as indicated by the Z_{cr} value varied substantially across hypotheses and across differing landmark densities. These Z_{cr} scores (Adams & Collyer, 2019; Table 2) indicate that, regardless of the density of the landmark data set used, the strongest signal of modular evolution was under the BKBR2 hypothesis. This two-module hypothesis separates the beak from the remaining portions of the skull and differs from the BKBR1 hypothesis in that cranial elements that are biomechanically linked to the beak (quadrates and jugals) are retained in the braincase module under the BKBR2 hypothesis. The Z_{cr} score for the BKBR1 hypothesis always received the second most negative score. Among other hypotheses, the FG5 hypothesis was universally recovered as having the weakest modular signal (as indicated by the least negative Z_{cr} scores). While the CR values remained relatively static across differing landmark densities, landmark density did relate to the variation in the strength of modular signal over all hypotheses as our densest landmarking scheme returned a higher range of Z_{cr} scores (16.701) relative to when we used our lowest density landmark set (a range of 4.53).

When support for each of these hypotheses relative to one another was compared via paired effect sizes (Figure 5), we recovered variable results (Figure 5). All hypotheses are strongly preferred ($p < .05$) over the null model of no modularity, regardless of landmark density. When the various versions of the FG hypothesis were compared to one another, very few significant differences were found, the exceptions being support for FG8 over FG4 and FG6 in the intermediate density analyses. Significant support for the two beak and braincase hypotheses, particularly for BKBR2, relative to the FG hypotheses was more frequent but not universal across all landmark densities. Across all densities, distinct support for one beak and braincase hypothesis over the other could not be discriminated ($p > .05$) on the basis of pairwise effect sizes.
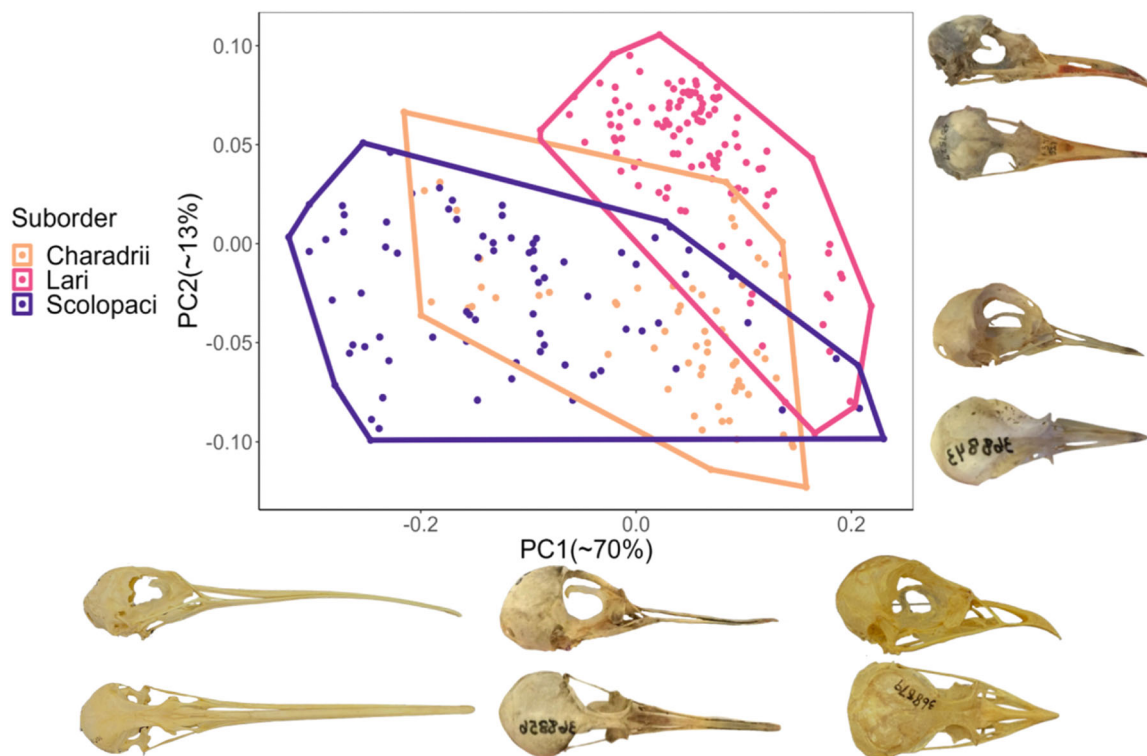
FIGURE 4 The results of a principal components analysis on 255 3D landmarks from the skulls of 262 different charadriiform species. Each point represents a species morphology digitized from three-dimensional surface scans from 1 to 2 museum specimens. Each of the three suborders (Charadrii, Lari, and Scolopaci) is encoded by color. Representative examples of changes along each of the first two principal components (explaining about 70% and 13% of overall shape variation, respectively) are shown on the *x* and *y* axis. Species shown along the *x* axis, listed left to right: long-billed curlew (*Numenius americanus*, FMNH 106289), common sandpiper (*Actitis hypoleucos*, FMNH 368856), and the collared pratincole (*Glareola pratincola*, FMNH 368879). Species along the *y* axis, listed top then bottom: Inca tern (*Larosterna inca*, FMNH 437577) and three-banded plover (*Charadrius tricollaris*, FMNH 368844).

3.3 | Testing for variable patterns of modular evolution across charadriiform subgroups

We recovered distinct CR values and Z_{cr} scores for the two subgroups relative to our analyses across all Charadriiformes (Figure 6). In the Lari, CR values skewed lower (all <0.75) while all CR values skewed higher (all >0.90) in our combined Charadrii + Scolopaci subgroup, suggesting skull modules evolve in a less correlated fashion in the Lari, relative to the Charadrii + Scolopaci. The Z_{cr} scores for each of the modularity hypotheses also varied between the two subgroups but were again universally more negative (indicating stronger support) in both subgroups relative to a null hypothesis of no modularity.

The FG4 hypothesis, in which the upper part of the beak and braincase are treated as a single module, received the least negative value (indicating the weakest support) in both subgroups. The most negative Zcr score (indicating the hypothesis with the strongest support) varied between the two families with the BKBR2 hypothesis receiving the most negative scores (similar to our findings at the ordinal level) in the Charadrii + Scolopaci while the FG8 hypothesis, the most finely subdivided of our hypotheses, received the most negative score within the Lari.

Pairwise comparisons of these Z_{cr} scores revealed complex relationships between support for the hypotheses when compared to one another (Figure 7). In both subgroups, all modularity hypotheses were significantly better ($p < .05$) than a null model of no modularity, with the exception of the FG5 hypothesis in the Charadii + Scolopaci suborder. Aside from these significant comparisons to the null hypothesis, significant differences in support were (similar to our order level results) recovered most frequently for comparisons between the FG hypotheses and the two versions of the beak and braincase hypothesis. Although the FG8 hypothesis was the most strongly supported within Lari (Figure 6, as indicated by the lowest effect size) it is only a significantly more supported hypothesis relative to the FG4 hypothesis for this clade. While the two beak and braincase hypotheses were significantly more supported over a larger number of hypotheses (Figure 7a), a significant difference in support for one of the beak and braincase hypotheses relative to the other was not recovered in the Lari (Figure 7a). Both the BKBR1 and 2 hypotheses received significantly stronger ($p < .05$) support than many of the FG hypotheses in the Charadii + Scolopaci (Figure 7b), and the two hypotheses were found to be distinctly supported from one another in this subgroup, with the BKBR2 hypothesis receiving a particularly negative Z_{cr} score of −16.38 (Figure 6).
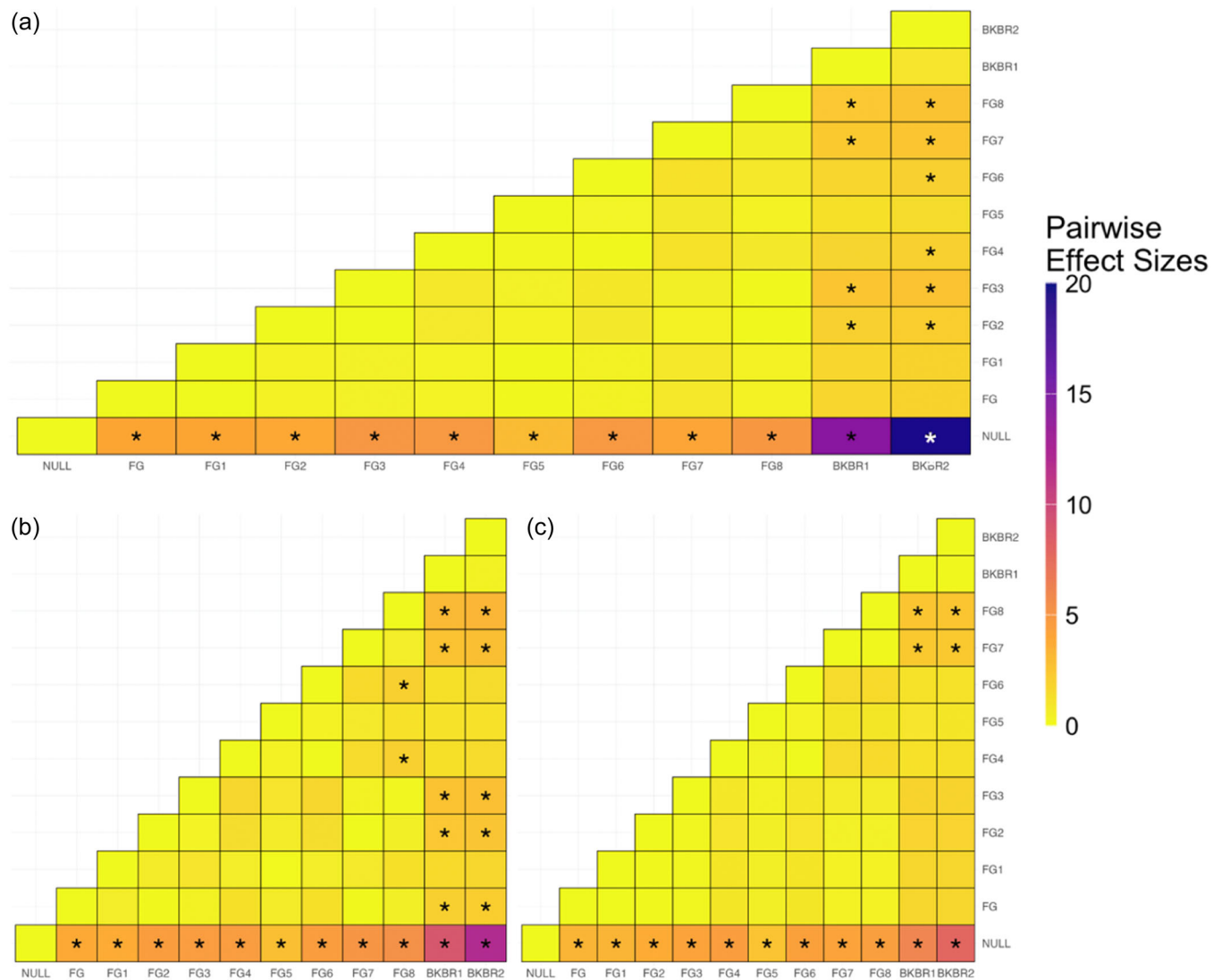
FIGURE 5 Support at the ordinal level for each modularity hypothesis for charadriiform skull evolution when analyzed using the full (a), intermediate (b), and low (c) density landmark set. Each hypothesis is indicated on the x axis with an abbreviation (see Table 1 and Figure 2). The pairwise difference effective size is denoted by the color of each cell with a black or white asterisk (distinct colors are used for increased readability) denoting significantly ($p < .05$) different support for that given pair of hypotheses. For these pairwise differences, we determined which hypothesis was favored by comparing the effect sizes (Figure 2) with the more negative value indicating the preferred hypothesis. NULL indicates the null model of no modularity to which the others were compared.

4 | DISCUSSION

In an effort to understand the patterns characterizing the morphological evolution of the vertebrate skull, hypotheses of modular evolution have been tested in a number of clades (Adams & Collyer, 2019; Bardua et al., 2019; Goswami & Finarelli, 2016; Klingenberg & Marugán-Lobón, 2013), using a variety of statistical methods (e.g., Adams & Collyer, 2019; Goswami & Finarelli, 2016). After quantifying the major axes of skull shape variation in a diverse order of birds, the Charadriiformes, we evaluated the support for 11 distinct hypotheses of modular evolution using morphometric data from the skulls of 262 different charadriiform species. We found that, while the density of landmarks used affected the magnitude of the

signal detected, the charadriiform skull has likely evolved in a modular manner, with the beak evolving semi-independently from the rest of the skull. Our subgroup-level analyses suggest this broad pattern of evolution is largely driven by one subgroup (the Charadrii + Scolopaci). Comparisons of this subgroup with another, more morphologically distinct subgroup (the Lari) suggest ecological differences between clades may be driving clade-specific patterns. In general, our results highlight important considerations for analyses of the modular evolution of the avian skull and, by investigating clade-specific results, suggest a framework for future research on the relationship between modularity, morphology, and ecology.

Our rejection of a null model of no evolutionary modularity stands in apparent contrast to previous findings based on birds of
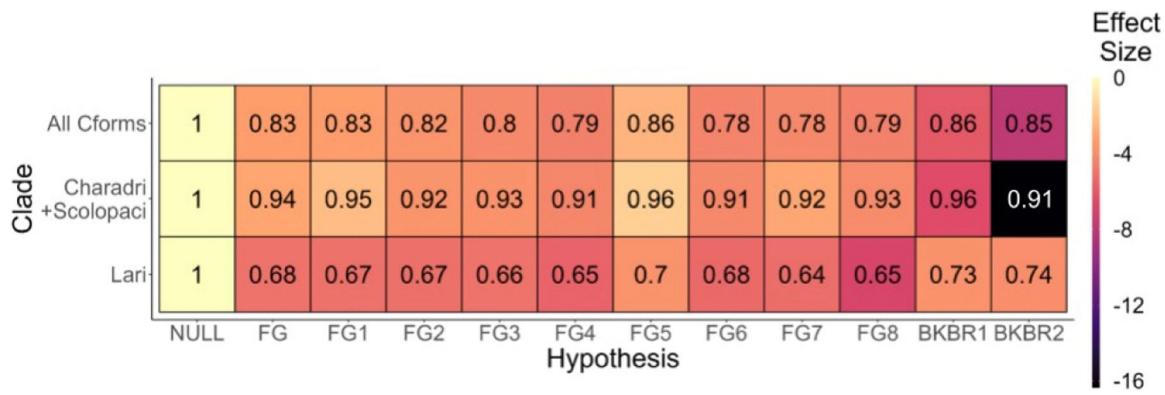
FIGURE 6 The covariance ratio (CR) values and effect sizes (Z_{cr} scores) for different modularity hypotheses across the charadriiform order ('All Cforms') as well within two different charadriiform subgroups: the Lari and a subgroup of the combined suborders Charadrii and Scolopaci ('Charadrii+ Scolopaci'). The CR value is indicated by the text in each cell, with values closer to 1 indicating a stronger degree of covariation between each pair of modules under that hypothesis. p values for these CR values are not labeled here but we note that all were <.05, indicating significant support for these hypotheses relative to a null model. The effect size (Z_{cr} scores), given by the color of each cell, demonstrates the relative support for that hypothesis, with more negative values indicating a higher modular signal (and therefore higher support) being detected under that hypothesis. Each hypothesis is indicated on the x axis with an abbreviation (see Table 1 and Figure 2). NULL indicates the null model of no modularity to which the others were compared.
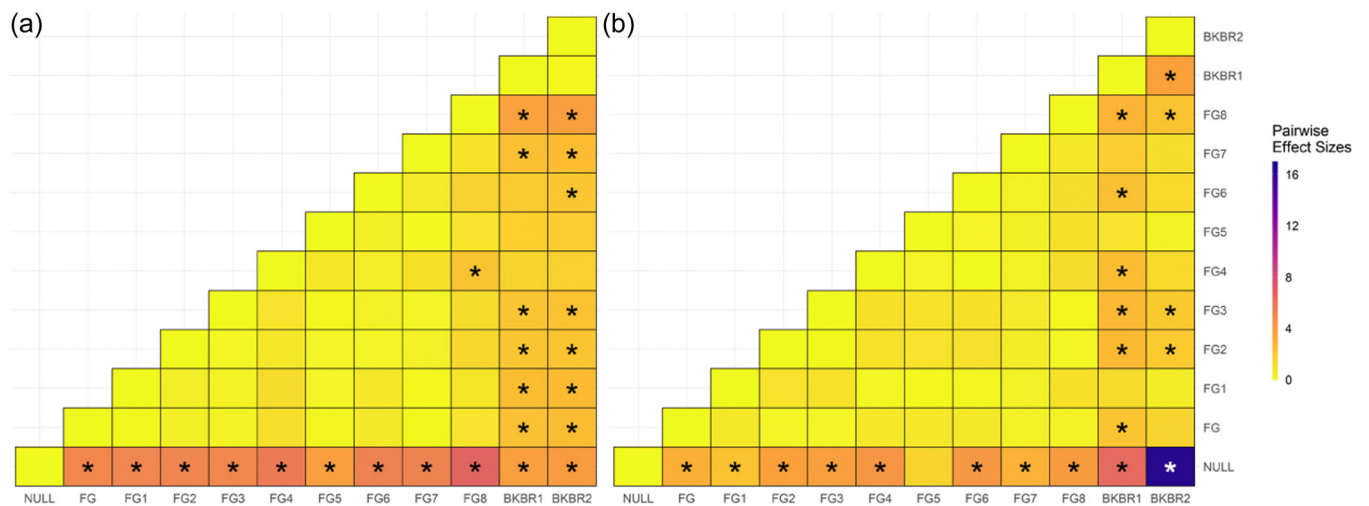

FIGURE 7 Pairwise effect sizes demonstrating variable support for modularity hypotheses for two different subclades: (a) the Lari and (b) a combined subgroup of the Charadrii + Scolopaci. The pairwise difference is denoted by the color of each cell with a black or white asterisk (distinct colors are used for increased readability) denoting significantly ($p < .05$) different support for that given pair of hypotheses. For these pairwise differences, we determined which hypothesis was favored by comparing the effect sizes (Table 2) with the more negative value indicating the preferred hypothesis.

prey (Bright et al., 2016), parrots (Bright et al., 2019), corvids (Kulemeyer et al., 2009), and across a broad sample of all birds (Klingenberg & Marugán-Lobón, 2013) that found evidence for correlated evolution between the beak and the braincase. These studies have relied on methods (Partial Least Squares; Bright et al., 2016, 2019; Kulemeyer et al., 2009 and the RV coefficient; Klingenberg & Marugán-Lobón, 2013) that assess the evidence for significant correlations between predefined modules. Considering the differing approach of these methods and of that used here (Adams & Collyer, 2019), our results are not incongruous with the idea that the skull has evolved in an integrated manner as these previous studies

have suggested. In agreement with these previous findings, our analyses all returned relatively high CR values (across all analyses were >0.64) indicating a substantial degree of integration between hypothesized modules. However, our results differ from several of these past studies (Bright et al., 2016, 2019; Kulemeyer et al., 2009) in that they include both explicit comparisons of distinct modularity hypotheses relative to one another and a quantifiable measure of the degree of integration between modules, allowing us a more nuanced understanding of the degree of modular evolution occurring. A similar pattern, a degree of modularity with notable integration between modules, was also recovered in a study on domestic dog skull

evolution that relied on calculations of RV coefficients (Drake & Klingenberg, 2010). Drake and Klingenberg (2010) recovered a degree of integration between the face and remaining portions of the skull, but still found significant support for modular evolution between these two elements. It is notable that a methodologically similar study on a broad sample of bird skulls by (Klingenberg & Marugán-Lobón, 2013), found evidence for integration between the beak and braincase as well and rejected a hypothesis of skull modularity. We suggest, given that we found the strongest support for a hypothesis that separated out the beak and braincase, the differing results between our study and that of Klingenberg and Marugán-Lobón (2013) may be explained by their exclusion of the distal portions (roughly corresponding to half) of the beak from their analysis.

Unlike previous studies using methodologies similar to ours that allow for direct comparisons of support for modularity hypotheses, we found little support for complex modularity scenarios. The discrepancy between this finding and that of Felice and Goswami (2018), who suggested that the avian skull is defined by seven evolutionary modules may be explained by the aforementioned tendency of the maximum likelihood method used to favor more complex modularity hypotheses (Adams & Collyer, 2019), a finding that is echoed in research using this method (Bardua et al., 2020; Conith et al., 2020, 2022; Goswami & Finarelli, 2016; Marshall et al., 2019; Mitchell et al., 2021). It is, however, notable that some authors (e.g., Mitchell et al., 2021) have found consistent results between this maximum likelihood method and CR method, suggesting that in certain species a high number of semi-independent modules may be a genuine pattern. While our finding that reducing the density of semi-landmarks did not typically affect significance testing may suggest landmark density is not of concern, the extreme Z_{cr} scores found when we used our highest density landmark set suggest extremely dense landmark placement could cause spurious results. This suggestion is in agreement with that of Goswami et al. (2019) who noted that semi-landmarks tend to exaggerate modularity (specifically within region integration and between region modularity). In particular, we relied heavily on semilandmarks placed along the skull's midline. This may have resulted in an over-estimation of correlated evolution between detected modules as global elongation along this axis of the skull may be the prominent signal detected in modularity analyses, thus obscuring more fine scale patterns.

It is possible that the lack of support for higher degrees of modularity in our work, as compared with Felice and Goswami (2018), may reflect the fact that they placed dense semi-landmarks on regions of the skull (e.g., in many neurocranial structures) that we did not. In particular, our inability to include small, detailed morphological structures (e.g., fossa glandulae nasalis) that cannot be reliably found across our data set may have led to a failure to detect more fine-scale modularity patterns within broader structures such as the neurocranium. While we were unable to test how this may have impacted our results, future research using micro-CT data could be used to test how the degree of detail in landmark placement may affect the modularity patterns recovered as the most supported. In general, our methodological choices (i.e., both in method of scanning used and in landmarking scheme) relative to past studies highlight the need for future research to carefully consider methodological choices such as landmark placement, density, and subdivision into hypothesized modules as well as the specific hypothesis testing method used.

Our subgroup level results and the spread of the three charadriiform suborders in our morphospace, however, point to levels of taxonomy as another potential reason for variation in past results. The extremely low Z_{cr} scores for both the BKBR1 (Z_{cr} score of −8.47) and BKBR2 (Z_{cr} score of −16.38) hypothesis in our Charadii + Scolopaci subgroup suggest that the species in that group may be the primary drivers of support for these two hypotheses at the ordinal level. Charadii+Scolopaci contain previously studied species where the notable diversity in skull morphology has been tied to foraging ecology (Natale & Slater, 2022). The skulls of both Charadii and Scolopaci species were found to primarily differ in terms of length and width, often being extremely long and thin (a morphology which is known to facilitate foraging into soft sediments Moreno, 1999; Zweers & Gerritsen, 1996). It is unsurprising that if beak lengthening is common in the evolution of these species, as suggested by our principal components analysis and by Moreno, (1999), our analyses would detect such strong support for the beak evolving as a semi-independent module.

However, it is noteworthy that even under both BKBR hypotheses, the CR values were quite high (>0.9), suggesting that the modularity between the beak and braincase, while significant, is low. Navalón et al. (2020) note through a modularity analysis on two notable adaptive radiations–the Hawaiian Honeycreepers and the finches of the Gal'apagos–that integration between modules may also drive adaptive radiation, as has been suggested in theoretical work (Villmoare, 2013). Further analyses explicitly connecting ecology to modularity are needed in the Charadii + Scolopaci suborder to confirm our hypothesis, but our results here in light of that of Moreno, (1999) and Zweers and Gerritsen (1996) suggest that the correlated, but still semi-independent, evolution of the beak with the remaining portions of the skull in this clade may help facilitate diversification of the skull morphology along an axis where length and width change in a correlated manner.

Our results in the Lari subgroup provide an interesting contrast to the Charadii + Scolopaci as we recovered a much less clear signal of support for any given hypothesis within this subgroup. It is notable the CR values recovered were universally lower in the Lari relative to the Charadii + Scolopaci, suggesting that under any given hypothesis, hypothesized modules tended to evolve more independently from one another. The Lari suborder is diverse containing species that differ substantially in ecology and skull morphology, although they tended to occupy more restricted areas of morphospace relative to the Charadii + Scolopaci. The majority of the suborder comprises species such as gulls, auks, and terns, that tend to forage through a variety of diving behaviors (del Hoyo et al., 1996), but the suborder also contains several small genera such as Turnicidae (buttonquails) and Glareolidae (coursers and pratincoles) that feed terrestrially or aerially. While it is known in this suborder that foraging ecology also relates strongly to skull shape (Natale & Slater, 2022) and there have been species-level analyses of adaptations for various behaviors in

both Lari (Zusi, 1962) and in ecologically similar species (e.g., other diving species Eliason et al., 2020), how changes in the morphologies of various skull components such as beak length or eye width may facilitate specific ecological behaviors (e.g., surface diving, pursuit diving, etc…) is not well understood on a macroevolutionary scale. It is possible that a more decoupled evolution of skull components, as suggested by our analysis, may relate to the ecological diversity in this group, but again a more explicit analysis analyzing how modular shape change, ecology, and the breadth of skull morphologies in this order relate to one another is needed.

Similar to our analyses and that of Navalón et al. (2020) who performed an in-depth exploration into a hyperdiverse clade, we encourage future covariance-ratio-based research into other avian clades that have been shown to exhibit great variation in foraging ecology and skull morphology such as Order Gruiformes (rails, cranes, and relatives; Livezey, 1998) and Procellariiformes (albatrosses, petrels, and relatives; Mazzochi & Carlos, 2022). An interesting contrast between studies in hyperdiverse clades such as these, studies on smaller, less disparate clades (e.g., corvids: Kulemeyer et al., 2009; parrots and cockatoos: Bright et al., 2019), and studies looking across all birds broadly (e.g., Felice and Goswami, 2018) may be drawn. Comparing the complexity of the modularity hypotheses that is found to be most supported to the ecological diversity within the clade studied would provide fruitful insight into the interplay between ecology, taxonomic scale, and the modular evolution.

5 | CONCLUSION

Contrary to previous research that has suggested the avian evolution has been characterized either by the skull evolving in one integrated unit or as a series of many anatomically distinct modules, we found support for the evolution of the beak and the rest of the skull evolving as two semi-independent modules throughout charadriiform evolution. We found this result to be robust to the use of different density landmark datasets, although our finding that the magnitude of the modular signal detected depended on landmark density highlights this as an important consideration in future research. We found this strong signal of modular evolution appeared to be driven by one subgroup (the Charadii + Scolopaci), which are known to have particularly diverse skull morphologies that relate to differences in foraging behavior. Future analyses investigating these results in light of variation in foraging mode may help elucidate the reasons for variation between subgroups and highlight broad macroevolutionary patterns of avian skull shape evolution. In general, we suggest future modularity research highlights clade-specific dynamics as they relate to differences in the ecology within and between clades.

AUTHOR CONTRIBUTIONS

Xiaoni Xu and Rossy Natale should be considered joint first authors. Xiaoni Xu and Rossy Natale both equally contributed to project conceptualization, data analysis, manuscript preparation, editing, and figure creation.

CONFLICT OF INTEREST STATEMENT

The authors have no conflicting interests to declare.

DATA AVAILABILITY STATEMENT

All data used in these analyses as well as the code used to conduct each analysis are available on Dryad (https://doi.org/10.5061/dryad. hmgqnk9n3). These analyses also relied on two previously published datasets available at (https://doi.org/10.5061/dryad.pc866t1p0) and (https://doi.org/10.5061/dryad.xksn02vjc), with the raw surface scan data available on morphosource (morphosource project ID: 00000C909).

ORCID

Xiaoni Xu https://orcid.org/0009-0007-6334-1442
Rossy Natale https://orcid.org/0000-0003-3055-3776

PEER REVIEW

The peer review history for this article is available at https://www.webofscience.com/api/gateway/wos/peer-review/10.1002/jmor.21703.

REFERENCES

Adams, D., Collyer, M., Kaliontzopoulou, A., & Baken, E. (2021). Geomorph: Software for geometric morphometric analyses. r package version 4.0.2.

Adams, D. C. (2016). Evaluating modularity in morphometric data: Challenges with the rv coefficient and a new test measure. *Methods in Ecology and Evolution*, 7(5), 565–572.

Adams, D. C., & Collyer, M. L. (2019). Comparing the strength of modular signal, and evaluating alternative modular hypotheses, using covariance ratio effect sizes with morphometric data. *Evolution*, 73(12), 2352–2367.

Baken, E. K., Collyer, M. L., Kaliontzopoulou, A., & Adams, D. C. (2021). geomorph v4.0 and gmshiny: Enhanced analytics and a new graphical interface for a comprehensive morphometric experience. *Methods in Ecology and Evolution*, 12, 2355–2363.

Bardua, C., Wilkinson, M., Gower, D. J., Sherratt, E., & Goswami, A. (2019). Morphological evolution and modularity of the caecilian skull. *BMC Evolutionary Biology*, 19(1), 30.

Bardua, C., Fabre, A. C., Bon, M., Das, K., Stanley, E. L., Blackburn, D. C., & Goswami, A. (2020). Evolutionary integration of the frog cranium. *Evolution*, 74(6), 1200–1215.

Benson, D. A., Cavanaugh, M., Clark, K., Karsch-Mizrachi, I., Lipman, D. J., Ostell, J., & Sayers, E. W. (2012). Genbank. *Nucleic Acids Research*, 41, D36–D42.

Bon, M., Bardua, C., Goswami, A., & Fabre, A.-C. (2020). Cranial integration in the fire salamander, *Salamandra Salamandra* (caudata: Salamandridae). *Biological Journal of the Linnean Society*, 130(1), 178–194.

Bright, J. A., Marugán-Lobón, J., Cobb, S. N., & Rayfield, E. J. (2016). The shapes of bird beaks are highly controlled by nondietary factors. *Proceedings of the National Academy of Sciences*, 113(19), 5352–5357.

Bright, J. A., Marugán-Lobón, J., Rayfield, E. J., & Cobb, S. N. (2019). The multifactorial nature of beak and skull shape evolution in parrots and cockatoos (psittaciformes). *BMC Evolutionary Biology*, 19(1), 104.

Černý, D., & Natale, R. (2022). Comprehensive taxon sampling and vetted fossils help clarify the time tree of shorebirds (Aves, Charadriiformes). *Molecular Phylogenetics and Evolution*, 177, 107620.

Chu, P. C. (1995). Phylogenetic reanalysis of strauch's osteological data set for the charadriiformes. *The Condor*, 97(1), 174–196.

Conith, A. J., Meagher, M. A., & Dumont, E. R. (2022). The influence of divergent reproductive strategies in shaping modularity and morphological evolution in mammalian jaws. *Journal of Evolutionary Biology*, 35(1), 164–179.

Conith, A. J., Kidd, M. R., Kocher, T. D., & Albertson, R. C. (2020). Ecomorphological divergence and habitat lability in the context of robust patterns of modularity in the cichlid feeding apparatus. *BMC Evolutionary Biology*, 20(1), 95.

Cooney, C. R., Bright, J. A., Capp, E. J. R., Chira, A. M., Hughes, E. C., Moody, C. J. A., Nouri, L. O., Varley, Z. K., & Thomas, G. H. (2017). Mega-evolutionary dynamics of the adaptive radiation of birds. *Nature*, 542(7641), 344–347.

Couly, G. F., Coltey, P. M., & Douarin, N. M. L. (1993). The triple origin of skull in higher vertebrates: a study in quail-chick chimeras. *Development*, 117(2), 409–429.

Drake, A. G., & Klingenberg, C. P. (2010). Large-scale diversification of skull shape in domestic dogs: Disparity and modularity. *The American Naturalist*, 175(3), 289–301.

Eliason, C. M., Straker, L., Jung, S., & Hackett, S. J. (2020). Morphological innovation and biomechanical diversity in plunge-diving birds. *Evolution*, 74(7), 1514–1524.

Felice, R. N., & Goswami, A. (2018). Developmental origins of mosaic evolution in the avian cranium. *Proceedings of the National Academy of Sciences*, 115(3), 555–560.

Felice, R. N., Randau, M., & Goswami, A. (2018). A Fly in a tube: Macroevolutionary expectations for integrated phenotypes. *Evolution*, 72(12), 2580–2594.

Goswami, A., & Finarelli, J. A. (2016). Emmli: A maximum likelihood approach to the analysis of modularity. *Evolution*, 70(7), 1622–1637.

Goswami, A., Watanabe, A., Felice, R. N., Bardua, C., Fabre, A.-C., & Polly, P. D. (2019). High-density morphometric analysis of shape and integration: The good, the bad, and the not-really-a-problem. *Integrative and Comparative Biology*, 59(3), 669–683.

Heesy, C. P. (2008). Ecomorphology of orbit orientation and the adaptive significance of binocular vision in primates and other mammals. *Brain, Behavior and Evolution*, 71(1), 54–67.

Klingenberg, C. P. (2008). Morphological integration and developmental modularity. *Annual Review of Ecology, Evolution, and Systematics*, 39(1), 115–132.

Klingenberg, C. P., & Marugán-Lobón, J. (2013). Evolutionary covariation in geometric morphometric data: Analyzing integration, modularity, and allometry in a phylogenetic context. *Systematic Biology*, 62(4), 591–610.

Kulemeyer, C., Asbahr, K., Gunz, P., Frahnert, S., & Bairlein, F. (2009). Functional morphology and integration of corvid skulls - a 3d geometric morphometric approach. *Frontiers in Zoology*, 6(1), 2.

Larouche, O., Zelditch, M. L., & Cloutier, R. (2018). Modularity promotes morphological divergence in ray-finned fishes. *Scientific Reports*, 8(1), 7278.

Livezey, B. C. (1998). A phylogenetic analysis of the gruiformes (aves) based on morphological characters, with an emphasis on the rails (rallidae). *Philosophical Transactions of the Royal Society of London. Series B: Biological Sciences*, 353(1378), 2077–2151.

Lowther, P. E., Diamond, A. W., Kress, S. W., Robertson, G. J., Russell, K., Nettleship, D. N., Kirwan, G. M., Christie, D., Sharpe, C., Garcia, E., & Boesman, P. F. D. (2020). Atlantic puffin (Fratercula Arctica). In Billerman, S.M., Keeney, B.K., P. G. Rodewald & T. S. Schulenberg, editors, *Birds of the World*. Cornell Lab of Ornithology.

Marshall, A. F., Bardua, C., Gower, D. J., Wilkinson, M., Sherratt, E., & Goswami, A. (2019). High-density three-dimensional morphometric analyses support conserved static (intraspecific) modularity in caecilian (amphibia: Gymnophiona) crania. *Biological Journal of the Linnean Society*, 126(4), 721–742.

Mazzochi, M. S., & Carlos, C. J. (2022). Skull morphology of four antarctic fulmarine petrels (aves: Procellariiformes): Insights into their feeding biology. *Polar Biology*, 45(2), 191–201.

del Hoyo, J., Elliot, A., & Sargatal, J. (Eds.). (1996). *Handbook of the birds of the World-From Hoatzin to Auks* (Vol. 3). Lynx Edicions.

Mitchell, M. J., Goswami, A., & Felice, R. N. (2021). Cranial integration in the ring-necked parakeet, *psittacula krameri* (psittaciformes: Psittaculidae). *Biological Journal of the Linnean Society*, 133(1), 47–56.

Moreno, E. (1999). Evolution of foraging strategies in shorebirds: An ecomorphological approach. *The Auk*, 116(3), 712–725.

Natale, R., & Slater, G. J. (2022). The effects of foraging ecology and allometry on avian skull shape vary across levels of phylogeny. *The American Naturalist*, 200(4), E174–E188.

Navalón, G., Marugán-Lobón, J., Bright, J. A., Cooney, C. R., & Rayfield, E. J. (2020). The consequences of craniofacial integration for the adaptive radiations of Darwin's finches and hawaiian honeycreepers. *Nature Ecology & Evolution*, 4(2), 270–278.

Olsen, A. M., & Westneat, M. W. (2016). Linkage mechanisms in the vertebrate skull: Structure and function of three-dimensional, parallel transmission systems. *Journal of Morphology*, 277(12), 1570–1583.

Paradis, E., Blomberg, S., Bolker, B., Brown, J., Claramunt, S., Claude, J., Cuong, H. S., Desper, R., Didier, G., Durand, B., Dutheil, J., Ewing, R. J., Gascuel, O., Guillerme, T., Heibl, C., Ives, A., Jones, B., Krah, F., Lawson, D., ...Vienne, D. d (2020). Ape: Analyses of phylogenetics and evolution. R package version 5.0.

Schlager, S. (2017). Morpho and rvcg – shape analysis in R. In Zheng, G., Li, S., and Szekely, G., editors, *Statistical Shape and Deformation Analysis* (pp. 217–256). Academic Press.

Stamatakis, A. (2014). RAxML version 8: A tool for phylogenetic analysis and post-analysis of large phylogenies. *Bioinformatics*, 30(9), 1312–1313.

Stratovan Corporation. (2018). *Stratovan Checkpoint*.

RStudio Team. (2019). *RStudio: Integrated Development Environment for R*. RStudio, Inc.

Vidal García, M., & Scott Keogh, J. (2017). Phylogenetic conservatism in skulls and evolutionary lability in limbs – morphological evolution across an ancient frog radiation is shaped by diet, locomotion and burrowing. *BMC Evolutionary Biology*, 17(1), 165.

Villmoare, B. (2013). Morphological integration, evolutionary constraints, and extinction: A computer simulation-based study. *Evolutionary Biology*, 40, 76–83.

Walker, J. A. (2000). Ability of geometric morphometric methods to estimate a known covariance matrix. *Systematic Biology*, *49*(10), 686–696

Watanabe, A., Fabre, A.-C., Felice, R. N., Maisano, J. A., Müller, J., Herrel, A., & Goswami, A. (2019). Ecomorphological diversification in squamates from conserved pattern of cranial integration. *Proceedings of the National Academy of Sciences*, *116*(29), 14688–14697.

Yang, Z. (2007). PAML 4: Phylogenetic analysis by maximum likelihood. *Molecular Biology and Evolution*, *24*(8), 1586–1591.

Zelditch, M., Swiderski, D., Sheets, H., & Fink, W. (2004). *Superimposition methods. In* geometric morphometrics for biologists (pp. 105–128). Elsevier.

Zelditch, M. L., & Goswami, A. (2021). What does modularity mean? *Evolution & Development*, *23*(5), 377–403.

Zusi, R. L. (1962). Structural adaptations of the head and neck in the black skimmer: *Rynchops nigra* (Linnaeus). *Publications of the Nuttall Ornithological Club*, *3*, 1–120.

Zweers, G. A., & Gerritsen, A. F. C. (1996). Transitions from pecking to probing mechanisms in waders. *Netherlands Journal of Zoology*, *47*(2), 161–208.

SUPPORTING INFORMATION

Additional supporting information can be found online in the Supporting Information section at the end of this article.